Load-driven morphological evolution in covalently bridged multiwalled carbon nanotubes

Xu Huang and Sulin Zhang[a)]
Department of Engineering Science and Mechanics, The Pennsylvania State University, University Park, Pennsylvania 16802, USA

(Received 26 February 2010; accepted 16 April 2010; published online 19 May 2010)

Under pure bending or compression multiwalled carbon nanotubes (MWCNTs) with interwall covalent bridges exhibit evolving morphologies, ranging from uniform deformation, wavelike rippling, to Yoshimura (diamond-shaped) pattern. Using large-scale coarse-grained simulations, we map out the morphological phase diagram in the space of applied strain and interwall bridging density and find that the three deformation phases are separated by two linear transition boundaries. Our energetics analyses reveal that the relative significance of the in-plane deformation energy and the interwall bridging energy determines the shape space of MWCNTs. The multiple morphological transformations open pathways for mechanically tuning the electronic and magnetic properties of MWCNTs. © *2010 American Institute of Physics*. [doi:10.1063/1.3428581]

Graphene shell exhibits large in-plane rigidity as compared to its bending rigidity,[1] and thus deforms nearly isometrically under external loading, featuring local sharp folds. Such deformation morphologies have been widely observed in previous studies: edge-induced warping in free-standing monolayer graphene;[2] local kinks in bent single-walled carbon nanotubes (SWCNTs);[3] beltlike structures in strongly twisted SWCNTs;[3] and the rippling or Yoshimura (diamond-shaped) patterns in twisted, bent, and compressed multiwalled carbon nanotubes (MWCNTs) with tens of walls or more.[4–13] These deformation phase transitions not only significantly reduce the rigidities of the thin shells but also alter their magnetic-electronic properties.[14,15] The morphological phase transitions are reversible upon unloading,[16–18] suggesting that these thin-shell structures may be designed as shape-memory devices with tunable stabilities.

In this letter, we report multiple morphological phase transitions in covalently bridged MWCNTs[19,20] under pure bending and uniaxial compression. The formation of bridged MWCNTs typically involves defects, and the mechanical properties of defected CNTs have been widely studied.[21–31] Typical interwall bridges include sp^3 bond involving an interstitial and sp^2 bond involving reconstructed single vacancies.[32,33] Both the covalent bonds provide a strengthening mechanism for MWCNTs that would otherwise have a rather low interwall shearing modulus.[34]

To improve computational affordability, we extend the coarse-grained model of Arroyo and Belytschko for carbon shells[35,36] by including the effects of interwall covalent bridges. In the extended model, the bonding interactions are described by the second-generation Brenner potential.[37] The interwall van de Waals (vdW) interactions are modeled by the Lennard–Jones potential.[38] To simplify our analysis, we restrict our discussion to the sp^3 bridged MWCNTs though the interwall bridges are in reality likely a combination of the sp^3 and sp^2 bonds.[39] The covalent bridges are treated as harmonic springs. From all-atom molecular dynamics simulations, the tensional and shear spring constants of the sp^3 bridge are k_n=43.31 aJ/nm^2 and k_τ=2.20 aJ/nm^2, respectively. The equilibrium and failure lengths of the sp^3 bridges are 0.28 nm and 0.52 nm, respectively. With given interwall bridge density ρ, defined by the number of excess interwall carbon atoms per unit cell of the hexagonal lattice of the graphene shells, the potential energy of these bridges can be homogenized into a continuum description in the manner similar to the treatment for the vdW interactions.[23,35] As compared to fully atomistic simulations using double-walled CNTs with interwall bridges, the extended coarse-grained model captures the atomistic energetics reasonably well and improves the computational efficiency by two orders of magnitude.

The mechanical responses of the covalently bridged MWCNTs subject to pure bending and uniaxial compression are studied. We adopt the ten-walled MWCNT, indexed by (5,5)/(10,10)/…/(50,50), as our simulation model. The constituent shells in the MWCNT are coarse-grained into finite elements, where the size effect of the elements is carefully examined to ensure numerical convergence. For pure bending, the four-point bending test[4] is performed, where

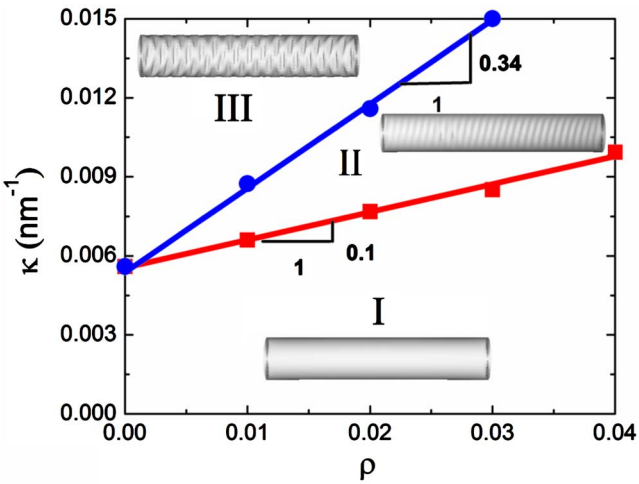

FIG. 1. (Color online) Morphological phase diagram of bent MWCNTs. I: uniformly deformed phase; II: rippling phase; and III: Yoshimura phase.

[a)]Author to whom correspondence should be addressed. Electronic mail: suz10@psu.edu.

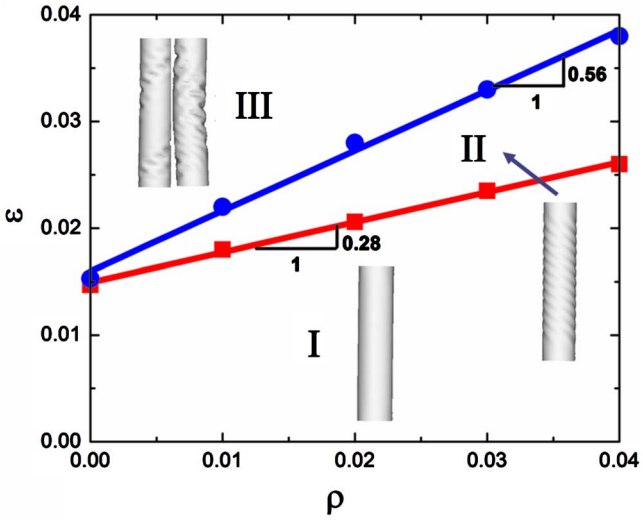

FIG. 2. (Color online) Morphological phase diagram of compressed MWCNTs. I: uniformly deformed phase; II: rippling phase; and III: Yoshimura phase.

four supplementary rigid short SWCNTs (two on the bottom, the other two on the top of the MWCNT) are used to bend the MWCNT. For uniaxial compression, the finite element nodes at the two ends of the MWCNTs are held fixed. Incrementally moving the fixed nodes at the two ends toward the center effectively compresses the MWCNT. For both loading cases, a limited-memory BFGS algorithm[40] is implemented to minimize the energy at each loading step, thereby finding the equilibrium configurations. The deformed configurations, reaction forces at the fixed nodes, and the in-plane and interwall interaction energies are all recorded at each loading step.

Figure 1 shows that under pure bending, the bridged MWCNT exhibits three morphological phases in the plane of bending curvature κ (unit: nm^{-1}) and interwall bridge density ρ. At a fixed bridge density, for low bending curvatures, the MWCNT behaves as an elastic beam and is uniformly bent (phase I). When the bending curvature increases and reaches a critical value, wavelike periodic rippling pattern (phase II) appears. Such rippling pattern resembles that observed in twisted MWCNTs.[8] With further increased bending curvature, the rippling pattern transits into the Yoshimura pattern (phase III). The longitudinal views of the three characteristic morphologies on the bent side of the MWCNT are inserted in Fig. 1. The rippling pattern is absent in the nonbridged MWCNT (ρ=0); the uniformly deformed phase transits directly into the Yoshimura pattern at the critical curvature of 0.0056 nm^{-1}. Increasing the interwall bridge density effectively widens the curvature range within which ripping pattern appears. For either pattern, the critical curvature linearly scales with the interwall bridging density, giving rise to linear phase boundaries with the slopes of 0.1 and 0.34, respectively. The linear scaling manifests the strengthening effect of the interlayer bridges against structural instability.

Figure 2 shows the phase diagram of the bridged MWCNT under uniaxial compression, where the regimes of the uniformly deformed (I), rippled (II), and diamond or combined (III) phases are indicated in the space of the compressive strain ε and the interwall bridge density ρ. The phase transition boundaries are nearly linear, with slopes of 0.28 and 0.56, as indicated in the figure. Our previous studies of uniaxially compressed, nonbridged MWCNTs showed that the constituent shells of a compressed MWCNT buckle in a coordinated manner.[7] Due to the presence of the interwall covalent bridges, the coordinated nature of the buckling of the constituent shells is pronounced. For the nonbridged MWCNT, the instability strains for the rippling and diamond patterns are very close to each other. With increasing interwall bridge density, the instability strains for these two patterns increase linearly, similar to the linear phase boundaries in bent MWCNTs. Overall, the regime for rippling pattern is rather narrow. It should be noted that at large compressive strains, the rippling and diamond patterns coexist for bridged MWCNTs. While for nonbridged MWCNT, only helically arranged diamond pattern appears.

Using pure bending case as an example, we next elucidate the deformation energetics that governs the morphological phase transition. We decompose the total strain energy into the in-plane deformation energy and interwall interaction energy. From our simulation results we identify the two

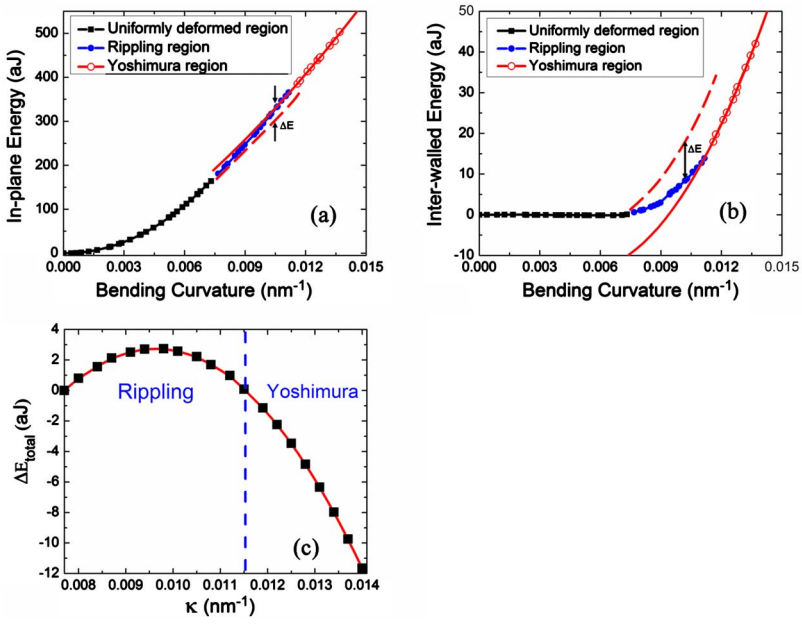

FIG. 3. (Color online) Energetics analysis of morphological phase transitions in the ten-walled MWCNT under pure bending. (a) In-plane strain energy and (b) interwall interaction energy. In (a) and (b), the energy curves for the uniformly deformed phase, the rippling phase, and the Yoshimura phase are, respectively, plotted by squares, filled and open circles connected by solid lines. The extrapolated segments from the energy curve of the Yoshimura phase downward to the rippling phases are shifted and plotted by dashed lines. (c) The total energy difference in the rippling and Yoshimura regimes.

phase transition points that separate the three deformation phases. The energy curves for these three phases are, respectively, plotted by squares, filled and open circles connected by solid lines, as shown in Figs. 3(a) and 3(b) (ρ=2%). We extrapolate the curve segments in the Yoshimura regime backward to the rippling regime [solid lines in Figs. 3(a) and 3(b)]. We then shift the extrapolated segment such that the extrapolated segment starts from the transition point from the uniformly deformed phase to the rippling phase. The shifted segments, marked by dashed lines in Figs. 3(a) and 3(b), correspond to the case as if the Yoshimura pattern would occur beyond the uniformly deformed phase. We found that the dashed segment is below the segment with filled circles in Fig. 3(a) but above in Fig. 3(b). This comparison suggests that if replacing the rippling pattern by the Yoshimura pattern at moderate curvatures, it would cause less in-plane strain energy, but larger interwall energy penalty. The total energy difference ($\Delta E_{\text{Total}}=E_{\text{Yoshimura}}-E_{\text{Rippling}}$) is plotted in Fig. 3(c). The energy difference in the rippling regime [left side of the dashed line in Fig. 3(c)] vanishes at the two phase transition points, and is always positive in between ($\Delta E_{\text{Total}} \geq 0$). This energetics analysis indicates that in the rippling regime the interwall bridging energy dominates the physics. In this regime, the Yoshimura pattern involves very high interwall energy penalty, and is thus energetically disfavored. We also extrapolate the energy curves of the rippling regime forward to the Yoshimura regime and compare accordingly the energetics. The total energy difference is always negative ($\Delta E_{\text{Total}} \leq 0$), and monotonically decreases in the Yoshimura regime, as plotted in Fig. 3(c) (right side of the dashed line). In this regime, the in-plane deformation energy dominates the physics. The rippling pattern involves much higher in-plane deformation energy than the Yoshimura pattern in this regime, and is thus energetically disfavored. We have also performed similar energetics analysis for the case of uniaxial compression and reached the similar conclusions.

In conclusion, our large-scale simulations observed multiple morphological deformation phases in bent and uniaxially compressed MWCNTs with interwall covalent bridges. We constructed phase diagrams in the plane of the applied strain and interwall bridging density for both loading cases. Our energetics analysis suggests that the morphological phase transition at different loading regimes is a result of interplay of the interwall interaction energy and the in-plane deformation energy. The multiple phase transitions in deformed MWCNTs not only influence the mechanical properties of the MWCNTs, but also alter their electronic-magnetic properties. Our study therefore opens pathways of tuning the electronic and magnetic properties of MWCNTs through mechanical deformations.

We gratefully acknowledge support from the National Science Foundation grant under Award No. 0600661.

[1]C. Lee, X. D. Wei, J. W. Kysar, and J. Hone, Science **321**, 385 (2008).
[2]V. B. Shenoy, C. D. Reddy, A. Ramasubramaniam, and Y. W. Zhang, Phys. Rev. Lett. **101**, 245501 (2008).
[3]B. I. Yakobson, C. J. Brabec, and J. Bernholc, Phys. Rev. Lett. **76**, 2511 (1996).
[4]M. Arroyo and I. Arias, J. Mech. Phys. Solids **56**, 1224 (2008).
[5]M. Arroyo and T. Belytschko, Phys. Rev. Lett. **91**, 215505 (2003).
[6]C. Bower, R. Rosen, L. Jin, J. Han, and O. Zhou, Appl. Phys. Lett. **74**, 3317 (1999).
[7]X. Huang, H. Y. Yuan, K. J. Hsia, and S. L. Zhang, Nano Res. **3**, 32 (2010).
[8]X. Huang, J. Zou, and S. L. Zhang, Appl. Phys. Lett. **93**, 031915 (2008).
[9]X. Y. Li, W. Yang, and B. Liu, Phys. Rev. Lett. **98**, 205502 (2007).
[10]A. Pantano, M. C. Boyce, and D. M. Parks, Phys. Rev. Lett. **91**, 145504 (2003).
[11]P. Poncharal, Z. L. Wang, D. Ugarte, and W. A. de Heer, Science **283**, 1513 (1999).
[12]J. Zou, X. Huang, M. Arroyo, and S. L. Zhang, J. Appl. Phys. **105**, 033516 (2009).
[13]I. Arias and M. Arroyo, Phys. Rev. Lett. **100**, 085503 (2008).
[14]T. W. Tombler, C. W. Zhou, L. Alexseyev, J. Kong, H. J. Dai, L. Lei, C. S. Jayanthi, M. J. Tang, and S. Y. Wu, Nature (London) **405**, 769 (2000).
[15]L. Yang and J. Han, Phys. Rev. Lett. **85**, 154 (2000).
[16]M. R. Falvo, G. J. Clary, R. M. Taylor, V. Chi, F. P. Brooks, S. Washburn, and R. Superfine, Nature (London) **389**, 582 (1997).
[17]S. Iijima, C. Brabec, A. Maiti, and J. Bernholc, J. Chem. Phys. **104**, 2089 (1996).
[18]A. Sears and R. C. Batra, Phys. Rev. B **73**, 085410 (2006).
[19]A. V. Krasheninnikov, K. Nordlund, and J. Keinonen, Phys. Rev. B **65**, 165423 (2002).
[20]D. T. Colbert, J. Zhang, S. M. McClure, P. Nikolaev, Z. Chen, J. H. Hafner, D. W. Owens, P. G. Kotula, C. B. Carter, J. H. Weaver, A. G. Rinzler, and R. E. Smalley, Science **266**, 1218 (1994).
[21]S. L. Mielke, D. Troya, S. L. Zhang, J. L. Li, S. P. Xiao, R. Car, R. S. Ruoff, G. C. Schatz, and T. Belytschko, Chem. Phys. Lett. **390**, 413 (2004).
[22]S. L. Zhang, R. Khare, Q. Lu, and T. Belytschko, Int. J. Numer. Methods Eng. **70**, 913 (2007).
[23]S. L. Zhang, S. L. Mielke, R. Khare, D. Troya, R. S. Ruoff, G. C. Schatz, and T. Belytschko, Phys. Rev. B **71**, 115403 (2005).
[24]S. L. Zhang, T. Zhu, and T. Belytschko, Phys. Rev. B **76**, 094114 (2007).
[25]S. L. Zhang, R. Khare, T. Belytschko, K. J. Hsia, S. L. Mielke, and G. C. Schatz, Phys. Rev. B **73**, 075423 (2006).
[26]T. Dumitrica, M. Hua, and B. I. Yakobson, Proc. Natl. Acad. Sci. U.S.A. **103**, 6105 (2006).
[27]S. L. Zhang and T. Zhu, Philos. Mag. Lett. **87**, 567 (2007).
[28]R. Khare, S. L. Mielke, J. T. Paci, G. C. Schatz, and T. Belytschko, Chem. Phys. Lett. **460**, 311 (2008).
[29]R. Khare, S. L. Mielke, J. T. Paci, S. L. Zhang, R. Ballarini, G. C. Schatz, and T. Belytschko, Phys. Rev. B **75**, 075412 (2007).
[30]S. L. Zhang, H. T. Johnson, G. J. Wagner, W. K. Liu, and K. J. Hsia, Acta Mater. **51**, 5211 (2003).
[31]T. Dumitrică, T. Belytschko, and B. I. Yakobson, J. Chem. Phys. **119**, 1281 (2003).
[32]A. Kis, G. Csanyi, J. P. Salvetat, T. N. Lee, E. Couteau, A. J. Kulik, W. Benoit, J. Brugger, and L. Forro, Nat. Mater. **3**, 153 (2004).
[33]R. H. Telling, C. P. Ewels, A. A. El-Barbary, and M. I. Heggie, Nat. Mater. **2**, 333 (2003).
[34]J. P. Salvetat, G. A. D. Briggs, J. M. Bonard, R. R. Bacsa, A. J. Kulik, T. Stockli, N. A. Burnham, and L. Forro, Phys. Rev. Lett. **82**, 944 (1999).
[35]M. Arroyo and T. Belytschko, J. Mech. Phys. Solids **50**, 1941 (2002).
[36]M. Arroyo and T. Belytschko, Phys. Rev. B **69**, 115415 (2004).
[37]D. W. Brenner, O. A. Shenderova, J. A. Harrison, S. J. Stuart, B. Ni, and S. B. Sinnott, J. Phys.: Condens. Matter **14**, 783 (2002).
[38]L. A. Girifalco, M. Hodak, and R. S. Lee, Phys. Rev. B **62**, 13104 (2000).
[39]Z. H. Xia, P. R. Guduru, and W. A. Curtin, Phys. Rev. Lett. **98**, 245501 (2007).
[40]D. C. Liu and J. Nocedal, Math. Program. **45**, 503 (1989).